Application of ion implantation as a tool to study neutron induced morphological changes in HOPG and RBMK-1500 reactor graphite

Elena Lagzdina, Danielius Lingis, Yves Pipon, Rita Plukienė, Ilja Ignatjev, Artūras Plukis, Nathalie Moncoffre, Gediminas Niaura, Vidmantas Remeikis

Contents lists available at ScienceDirect

Nuclear Inst. and Methods in Physics Research, B

journal homepage: www.elsevier.com/locate/nimb

Application of ion implantation as a tool to study neutron induced morphological changes in HOPG and RBMK-1500 reactor graphite

Elena Lagzdina [a,*], Danielius Lingis [a], Yves Pipon [b], Rita Plukienė [a], Ilja Ignatjev [c], Artūras Plukis [a], Nathalie Moncoffre [b], Gediminas Niaura [c], Vidmantas Remeikis [a]

[a] Department of Nuclear Research, Center for Physical Sciences and Technology (FTMC), Savanorių Ave. 231, LT-2300 Vilnius, Lithuania
[b] Univ Lyon, Univ Claude Bernard Lyon 1, CNRS/IN2P3, IP2I Lyon, UMR 5822, F-69622, Villeurbanne, France
[c] Department of Organic Chemistry, Center for Physical Sciences and Technology (FTMC), Saulėtekio Ave. 3, LT-10257 Vilnius, Lithuania

ARTICLE INFO

Keywords:
RBMK nuclear graphite
HOPG
Ion implantation
Raman spectroscopy
SIMS

ABSTRACT

Based on the RBMK-1500 *(rus.: реактор большой Мощности канальный, РБМК; reaktor bolshoy moshchnosti kanalnyy, "high-power channel-type reactor")* reactor irradiation conditions, ion implantation was used as a tool to study neutron induced morphological changes in both highly oriented pyrolytic graphite (HOPG) and nuclear grade RBMK graphite. Graphite samples were implanted with 180 keV $^{14}N^{+}$ ions at the fluences of 1.0×10^{16} ions/cm^{-2} and 2.5×10^{16} ions/cm^{-2}. To study temperature effects on both ion migration and structural disorder level in the graphite matrix, the implantation procedures were carried out under different temperature conditions – room temperature (RT) and 500 °C. Subsequently, the distribution profiles of the implanted $^{14}N^{+}$ ions were obtained by using secondary ion mass spectroscopy (SIMS) technique, while the microstructural properties of the graphite were evaluated by Raman spectroscopy. Implantation induced primary displacement damage profiles and implanted ion profiles were evaluated theoretically by using GEANT4 10.6 and SRIM-2013 codes. The profiles of implanted nitrogen obtained by SIMS technique were found to be in good agreement with theoretical ones. The surfaces of HOPG samples displayed macroscopic damage in form of fractures after $^{14}N^{+}$ ion implantation at 500 °C; however, in case of RBMK graphite, the sample surfaces remained without visually observable changes. The Raman spectra showed an increase of sp^3-related content and formation of amorphous carbon in both HOPG and RBMK graphite samples; the latter exhibits higher structural disorder at microscopic level and stronger amorphization than HOPG.

1. Introduction

The main problem when dealing with irradiated graphite waste management strategy is the radioactive content of different radionuclides which arises during the activation process from impurities, surface contamination or graphite matrix itself. One of the main contributors to the total activity of irradiated graphite is ^{14}C also known as radiocarbon. There are three different reactions which result in radiocarbon production in the nuclear graphite under reactor operational conditions: $^{14}N(n,p)^{14}C$, $^{13}C(n,\gamma)^{14}C$ and $^{17}O(n,\alpha)^{14}C$. However, the majority of ^{14}C is produced from isotope ^{14}N when capture of thermal neutrons occurs. ^{14}N is usually found as impurity in different concentrations up to 300 ppm depending on nuclear graphite type [1]. Despite the fact that RBMK type nuclear graphite is very pure material, it contains traces of nitrogen – average nitrogen concentration is 15 ppm, while maximum concentration can reach up to 70 ppm [2]. Moreover, the mixture of the helium-nitrogen gas (70–90 % He, 10–30 % N_2) circulates in the core of the RBMK reactor during its operation at an excess pressure of 0.49–1.96 kPa [3]. Nitrogen may adhere to outer surface of the graphite structural components via chemisorption and incorporate into material forming covalent bonds. The $^{14}N(n,p)^{14}C$ nuclear reaction results in ^{14}C atoms with the kinetic energy of 41.4 keV which is high enough to break any chemical bond. Continuous neutron irradiation induces point defects in the graphite matrix which tend to agglomerate and form extended defects if reordering process does not take place. These defects as well as any carbon atom with free valence electron in disordered graphite structures serve as the binding sites for ^{14}C in neutron irradiated nuclear graphite [1]. Therefore, the relatively high concentration of ^{14}N atoms in the reactor active zone during its operational time is located on the surfaces and/or in the near-surface

* Corresponding author.
E-mail address: elena.lagzdina@ftmc.lt (E. Lagzdina).

https://doi.org/10.1016/j.nimb.2023.02.024
Received 14 January 2022; Received in revised form 20 February 2023; Accepted 21 February 2023

structures of graphite constructions. The high level of structural disorder in the graphite material may lead to ^{14}N migration and its incorporation and stabilization as ^{14}C in the irradiated graphite matrix. The intensity of these processes may vary depending on graphite type, reactor type, operational parameters etc., therefore, the experimental graphite activation investigation should be performed in each case.

Nuclear grade graphite is an artificial material produced from pitch and petroleum coke grains under high temperature conditions which is also known as graphitization process. This process results in an heterogeneous material with binder matrix and coke filler particles. Due to this, nuclear grade graphite exhibits both areas of oriented morphology and extensive micro cracking [4]. The distribution of the pores and cracks depends on the choice of raw materials and manufacturing process. Grain size, as the main parameter for classification of the synthetic graphite, mainly depends on the size of filler particles. Both physical and mechanical properties of synthetic graphite depend on micro and macrostructure of crystals.

Ion implantation method is widely used as a tool to study neutron induced structural changes in graphite matrix under reactor operational conditions [5]. $^{12}C^+$ ion implantation as a tool to study structural changes in RBMK-1500 reactor graphite was used in [6]. HOPG as a form of high-purity synthetic graphite with a high degree of preferred crystallographic orientation, is often used as the reference material and model system for the single crystal graphite in such kind of studies [7,8]. Structural studies of both HOPG and RBMK graphite in coupled manner may provide insights about particularities of the morphological behavior of the nuclear graphite under reactor operational conditions. Moreover, the understanding of the morphological properties of the irradiated graphite is important for determination of the chemical form and stability of the radionuclides (especially ^{14}C) in the irradiated graphite matrix containing crystal grains and open pores. The aim of this work is to compare the structural behavior of both HOPG and nuclear grade RBMK graphite under different $^{14}N^+$ ion irradiation conditions – fluence and temperature. This is the first step in order to understand physicochemical processes of incorporation and stabilization of ^{14}C in the irradiated nuclear graphite.

2. Materials and methods

2.1. Sample preparation and ion implantation

Graphite samples were cut out from a raw graphite stack column of the RBMK-1500 reactor obtained from the Ignalina nuclear power plant (Ignalina NPP). The samples in dimensions around 10 × 10 × 5 mm were prepared for ion implantation experiments. HOPG was obtained from SPI Supplies (West Chester, US) through Neyco SA (Paris, France) in form of 1 mm thick 10 × 10 mm^2 plates. No additional surface treatment was applied before the ion implantation procedure. A batch of samples (1 sample of RBMK nuclear graphite and 1 sample of HOPG) was implanted with $^{14}N^+$ ions at the energy of 180 keV and a fluence of 1.0 × 10^{16} ions/cm^2, while another batch at a fluence of 2.5 × 10^{16} ions/cm^2. In this study the $^{14}N^+$ ion implantation conditions were chosen, taking into account the average amount of defects in the RBMK-1500 reactor which was calculated as high as 0.51 DPA/full power year. Theoretical evaluation of the primary displacement damage in the neutron irradiated RBMK-1500 graphite is described in details elsewhere [9]. The implantation procedure was carried out under vacuum (7 × 10^{-7} mbar) at the RT as well as temperature of 500 °C at the Pprime Institute, CNRS-Poitiers university, France.

2.2. SIMS measurements and depth profile estimation

To study the distribution profiles of the implanted $^{14}N^+$ ions SIMS experiments were carried out. Measurements were performed by using ION ToF-SIMS V equipment at SERMA Technologies, laboratory *Science et Surface*, Ecully, France. The focused primary beam was rastered over an area of 100 × 100 μm^2 on the sample surface. Secondary ions ($^{14}N^+$ and $^{12}C^+$) were collected from a smaller region (20 × 20 μm^2) located at the center of the sputtered area to minimize crater-edge effects. For each $^{14}N^+$ profile, the depth scale was determined by measuring the crater depth by optical interferometry with a Neox 3D interferometer of Sensofar. The experiments were carried out at the Laboratoire de Mécanique des Contacts et des Structures (LaMCoS) at the Institut National des Sciences Appliquées (INSA), Lyon, France. The nitrogen concentration was determined thanks to the use of the Relative Sensitive Factor (RSF) introduced by Wilson [10].

2.3. Ion beam interaction simulations

Implantation induced primary displacement damage profiles and implanted ion profiles were evaluated using GEANT4 10.6 [11] and SRIM-2013 (The Stopping and Range of Ions in Matter) [12] codes. Both GEANT4 and SRIM-2013 are Monte Carlo based simulation codes which use binary collision approximation (BCA) to obtain the displacement damage. In BCA, the interactions are treated as single atom-projectile pair events and the target lattice is simulated as being static (at 0°K). Moreover, there is no displacement damage accumulation during the simulations and the material is treated as amorphous. Although SRIM-2013 code is used as an industry standard in such calculations, GEANT4 code can also be used for the evaluations as it is a versatile simulation toolkit capable of simulating displacement and implantation profiles with great accuracy. Moreover, the comparison of results could provide insight on the expected experimental implanted atoms profiles. The main reason of GEANT4 usage in this research is the ability to use other than SRIM-2013 stopping powers. Additionally, the information about the individual recoils (energy, momentum direction, depth in the sample, etc.) can be obtained.

The SRIM-2013 and GEANT4 simulation tools were used for comparison of the implanted atom and the displacement intensity profiles. The projected range of implanted ions R_p indicates the average value of depth the incident particles will penetrate to. This value is measured along the initial direction of the impinging particles. When particle beam is perpendicular to the surface of the sample, the projected range of simulations can be easily compared to the SIMS depth results. The projected range values (see Table 1) also contain the error which is obtained from range straggling equation (1):

$$[(\sum_i x_i^2)/N - R_p^2]^{1/2} \quad (1)$$

here $\Sigma_i x_i^2$ is the sum of the squared range of individual ions, N is the number of particles simulated and R_p is the projected range of all ions, obtained from the simulations.

2.3.1. Ion beam interaction simulations with SRIM-2013 code

The ion beam interactions were numerically simulated for HOPG graphite (density 2.25 g/cm^3) and RBMK graphite (density 1.7 g/cm^3) by using SRIM-2013 toolkit. In SRIM-2013 environment, the Kinchin-Pease method was used for evaluations of both the implanted ion profile and the primary displacement damage profile. The implanted ion profile does not depend much on whether the Full-Cascades option or the Kinchin-Pease method is chosen. However, the primary displacement damage depends on the approach. The primary displacement damage estimated by using the Full-Cascades method is higher than compared to the Kinchin-Pease method and the difference depends on the target-ion pair. In this research the primary displacement damage was evaluated based on the recommendations by other authors (see [13;14]), namely, the Kinchin-Pease method with lattice binding energy set to 0 eV. The damage energy (energy of the ion that is dissipated in elastic collisions with the atoms of the lattice) is calculated based on energy lost to lattice phonons. To quantify the primary displacement damage, DPA (displacement per atom) units are used. DPA refers to the

Table 1
Comparison of the theoretical implantation values for HOPG and RBMK graphite when implanted with $^{14}N^{+}$ ions at the energy of 180 keV and fluence of 1.0 × 10^{16} ions/cm^2.

Graphite type	HOPG	RBMK
Density	2.25 g/cm^3	1.7 g/cm^3
Projected range of ions:		
SRIM-2013	300 ± 45 nm	397 ± 60 nm
SRIM-2013 CR[1]	336 ± 51 nm	440 ± 68 nm
GEANT4 SR[2]	305 ± 45 nm	405 ± 60 nm
GEANT4 IC73[3]	328 ± 50 nm	434 ± 66 nm
GEANT4 IC90[4]	283 ± 41 nm	375 ± 54 nm
Maximum number of displacements per atom (DPA)		
SRIM-2013	1.51	1.14
SRIM-2013 CR	1.56	1.18
GEANT4 SR	1.8	1.37
GEANT4 IC73	1.77	1.34
GEANT4 IC90	1.84	1.39
Average number of defects on the surface (~50 nm) (DPA)		
SRIM-2013	**0.41**	**0.4**
SRIM-2013 CR	**0.42**	**0.4**
GEANT4 SR	**0.77**	**0.76**
GEANT4 IC73	**0.76**	**0.75**
GEANT4 IC90	**0.77**	**0.76**
Average amount of defects in the nuclear reactor due to the neutron damage **(DPA/full power year)**	–	**0.51**

[1] SRIM-2013 with compound correction, [2]GEANT4 with SRIM stopping powers, [3]GEANT4 with ICRU73 stopping powers, [4]GEANT4 with ICRU90 stopping powers.

average number of times an atom is displaced from its original lattice site. The DPA rate is obtained by using the previously mentioned damage energy in the Norgett–Robinson–Torrens (NRT) [15] equation:

$$DPA = (0.8 \times T)/(2 \times E_d) \quad (2)$$

here T is the total damage energy, E_d is the threshold energy to create a displacement (displacement energy) which was set to 25 eV in this research. Vacancy production profiles (from VACANCY.txt file) were modified by the ratio of number of vacancies obtained by simulation (from summing vacancies produced by both ions and recoils, from VACANCY.txt file) to the number of vacancies obtained from (1) formula. By using the NRT method, the number of vacancies obtained is by a factor of 1.067 larger than obtained from SRIM-2013 Full-Cascades simulations. The displacement damage profile (vacancies per angstrom per ion) is multiplied by this factor to obtain the NRT based displacement profile. The implanted ion profiles and displacement damage profiles were simulated with two material setups: one with a compound correction and one without it. The compound correction in SRIM-2013 essentially alters the elemental stopping powers due to different outer shell electron orbitals when compared to the elemental material [16]. In the case of our research the nitrogen ion-graphite pair gives a compound correction of 0.868 and by 13.2% lower stopping powers.

2.3.2. Ion beam interaction simulations with GEANT4 toolkit

GEANT4 is an open-source toolkit written in C++ and designed for the simulation of particles traversing the matter. GEANT4 provides an extensive possibility to use different physics lists and processes. In this research, the simulation process was made by including several physics processes. For simulation of electronic energy loss of ions, the *G4ionIonisation class* was used with step function parameters 0.1, 0.02 mm. The *G4ionIonisation class* uses *G4BraggIonModel* for low energy ions and *G4BetheBloch model* for high energy ions. However, for low energy ions *G4IonParametrisedLossModel model* can be used which allows simulating energy loss based on the stopping power parametrization or experimental values for materials defined in ICRU73 [17] or ICRU90 [18] stopping power libraries. ICRU73 (*Stopping of Ions Heavier Than Helium*) library does not contain stopping powers for graphite material and uses parametrization based on carbon atoms, while ICRU90 (*Key Data For Ionizing-Radiation Dosimetry: Measurement Standards And Applications*) library contains stopping powers of graphite. Moreover, *G4IonParametrisedLossModel* was modified to allow the usage of SRIM stopping powers. The material used in the simulations was G4_Graphite with a density set to 2.25 g/cm^3 for HOPG and 1.7 g/cm^3 for RBMK graphite. For scattering events, the single scattering class *G4CoulombScattering* with *G4IonCoulombScatteringModel model* was used. The recoil threshold energy was set to 25 eV. The nuclear energy loss was simulated with the *G4NuclearStopping class* which uses ICRU49 (*Stopping powers and ranges for protons and alpha particles*) [19] stopping powers. ICRU49 reported stopping powers can deviate by 10 – 20 % for lower energies when compared to SRIM-2013 stopping powers, thus, a deviation in range and primary displacement damage is also expected [20]. The nuclear energy loss was obtained by using *G4NIELCalculator method* which evaluated non-ionizing energy loss (NIEL) for each step of the particle. The total NIEL energy was used in equation (2) with a 25 eV displacement energy to obtain the total number of displacements per ion. For comparison reasons the primary displacement damage and implanted ion profiles obtained with GEANT4 toolkit were evaluated based on the ICRU73, ICRU90 and SRIM electronic stopping powers.

2.4. Raman spectroscopy

The graphite samples were characterized by Raman spectroscopy in ambient conditions using a Renishaw inVia spectrometer. The excitation light of 532 nm was used. The laser beam was focused using 50 × objective lens to a 0.8 μm diameter spot on the sample surface. A very low incident power of about 0.3 mW was used to avoid the heating effect. Spectra were acquired from 3 to 5 areas of each sample, while each individual spectrum was collected over 100 s. All the spectra were registered in the Raman shift range from 1000 to 3000 cm^{-1}. Before and after the measurements, a silicon sample spectrum was acquired and a 520.7 cm^{-1} peak was used for wavenumber calibration.

3. Results and discussion

3.1. The nitrogen concentration profiles measured by SIMS

The distribution profiles of the implanted $^{14}N^{+}$ ions in both HOPG and RBMK nuclear graphite samples were obtained by SIMS at both fluences and temperatures. The nitrogen distribution profiles in HOPG samples are shown in Fig. 1.

For the higher implantation fluence (2.5 × 10^{16} N^{+}/cm^2), the entire depth profiles measured by SIMS are really close to the calculated ones. For the lower implantation fluence (1.0 × 10^{16} N^{+}/cm^2), the base signal measured by SIMS is high revealing a probable pollution during ion implantation as no nitrogen content is expected in HOPG samples. But, even if the depth profiles are higher than expected, we can rely on the R_p values. In all cases, the peak maximum measured by SIMS is at about 300 nm in good agreement with the calculated values by the MC codes. The SIMS technique has usually an excellent depth resolution (<10 nm) if the roughness is low which is the case for the HOPG samples (see Fig. 3, left). Therefore, we can assume a small shift of the peak towards the sample surface when implanted at 500 °C.

The nitrogen distribution profiles in RBMK graphite samples are shown in Fig. 2. It should be noted that for RBMK graphite the experimental peaks are much broader than simulated ones (and also than the depth profiles measured by SIMS in HOPG samples). This is explained by a high value of the surface roughness in RBMK graphite samples due to the structural non-homogeneity and the porosity of RBMK graphite (see Fig. 3, right). For this reason, the transformation of the SIMS sputtering

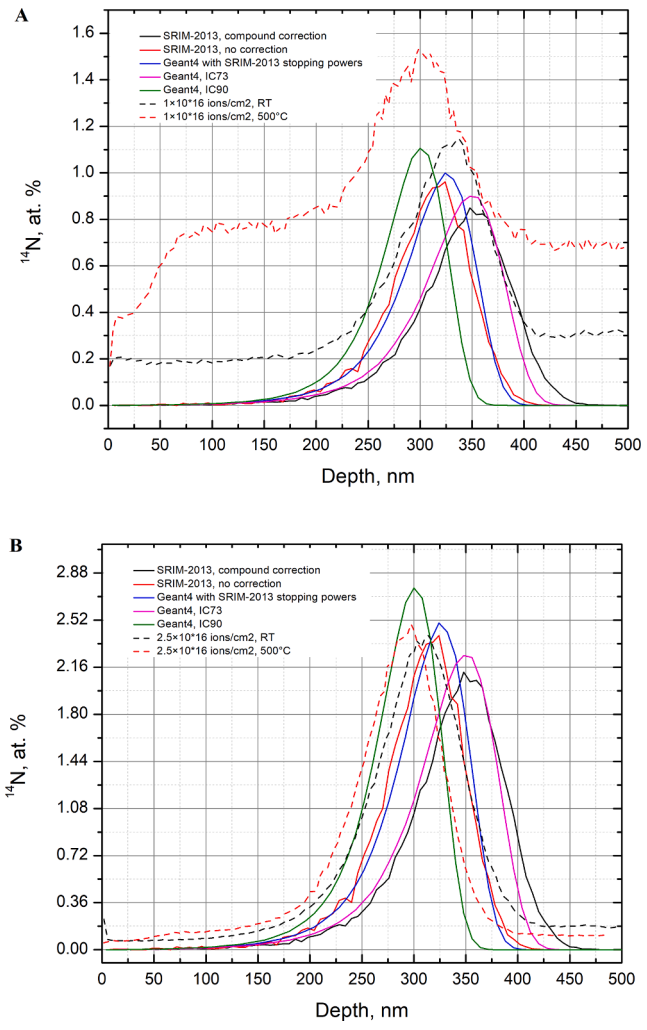

Fig. 1. The nitrogen distribution profiles in HOPG: (A) experimentally obtained in the samples implanted at a fluence of 1×10^{16} ions/cm^2 and compared to simulated ones; (B) experimentally obtained in the samples implanted at a fluence of 2.5×10^{16} ions/cm^2 and compared to simulated ones.

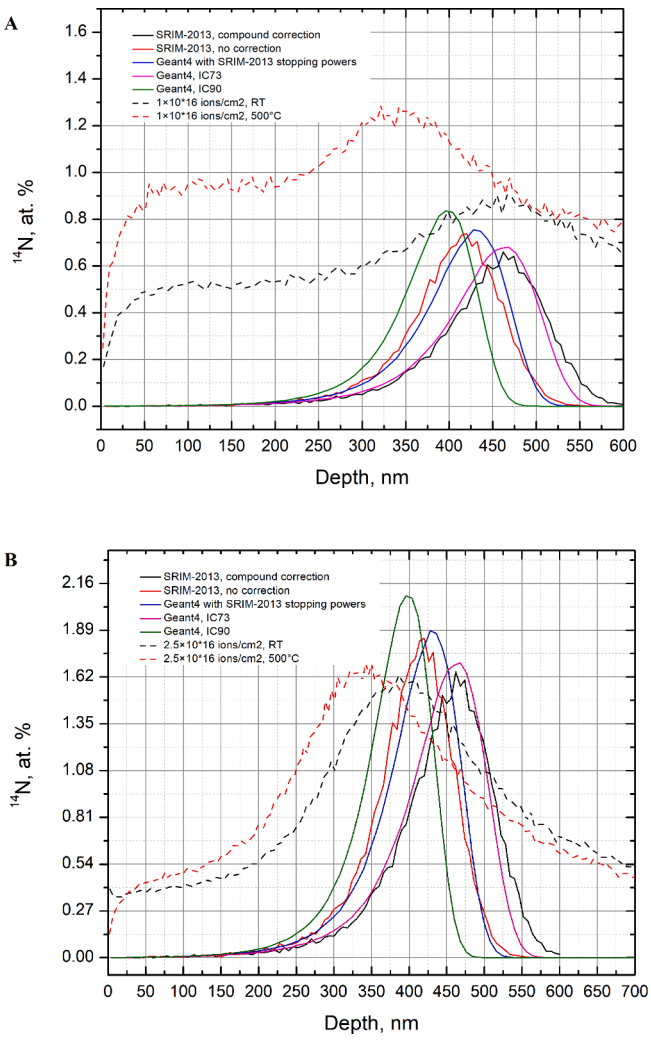

Fig. 2. The nitrogen distribution profiles in RBMK graphite: (A) experimentally obtained in the samples implanted at a fluence of 1×10^{16} ions/cm^2 and compared to simulated ones; (B) experimentally obtained in the samples implanted at a fluence of 2.5×10^{16} ions/cm^2 and compared to simulated ones.

time into depth leads to a huge error which can be estimated to be around 100 nm according to the crater roughness. Even with this error, it can be seen that the R_p measured by SIMS is around 400 nm in agreement with the calculated values. It can also be noted that: (i) the SIMS baseline shows a nitrogen concentration of around 0.4 and 0.5 % at. in RBMK graphite samples, and (ii) a same tendency of the peak shift towards the surface after implantation at 500 °C is likely to occur. In some cases, the surface region (0 to 10 nm) affected by the surface contamination and the tails of the profiles (<200 nm) affected by the 'knock-on' effect [21] were observed.

3.2. *Comparison of the nitrogen concentration profiles measured by SIMS and calculated by MC simulations*

The implantation induced primary displacement damage profiles and implanted ion profiles for both RBMK and HOPG graphite are shown in Fig. 4.

The comparison of HOPG and RBMK nuclear grade graphite properties is shown in Table 1. The modelling results of $^{14}N^+$ ion implantation at the energy of 180 keV and fluence of 1.0×10^{16} ions/cm^2 are also presentred. In the case of the fluence of 2.5×10^{16} ions/cm^2 the presented DPA values should be simply multiplied to 2.5. This is due to modelling limitations, especially, there is no damage accumulation during the simulation as every incident ion interacts with material which is not affected by previous ions. The more detailed description of the modelling limitations was described in [22].

HOPG is formed by oriented stacking of graphene planes, while nuclear grade RBMK graphite is heterogeneous material with high internal porosity. Porosity of GR-280 grade graphite is about 23 %, from which 17 % are for open and 6 % are for closed pores volume [23]. Previous studies on microstructure of the GR-280 graphite, from which the stack of the RBMK reactor is formed, report that the filler particles are in irregularly angled shape with the grain size of 0.5–1.5 mm. The size of crystal structures was found to be 10–20 μm. The binder material is reported as fine-grained crystallites of about 1 μm [3]. These microstructural particularities lead to the higher implantation depth when compared to HOPG.

As observed in HOPG, the maximum concentration of implanted nitrogen ions differs by about 53 nm when compared SRIM-2013 to GEANT4 results. The difference between peak positions is about 65 nm in the case of RBMK graphite. Another distinct difference is that the GEANT4 simulated peak is broader than obtained by SRIM-2013. This is due to the fact, that width of GEANT4 peak is smaller than the SRIM-2013 one. Although the GEANT4 simulated peak intensity is higher, the integrated concentration is equal between both codes. This means that GEANT4 simulated peak width is smaller. In the case of primary

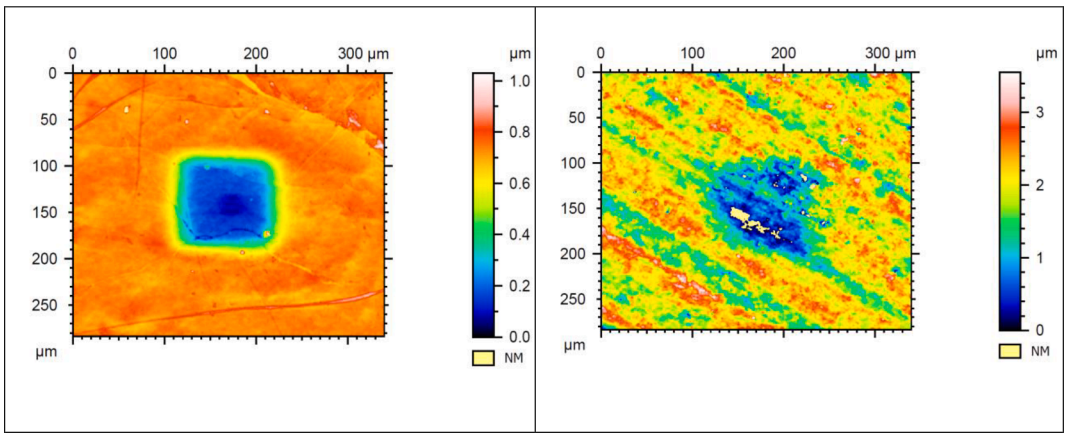

Fig. 3. SIMS craters in the HOPG (left) and RBMK graphite (right) sample surface after implantation with $^{14}N^{+}$ ions at the fluence of 2.5 × 10^{16} ions/cm^2 at temperature of 500 °C.

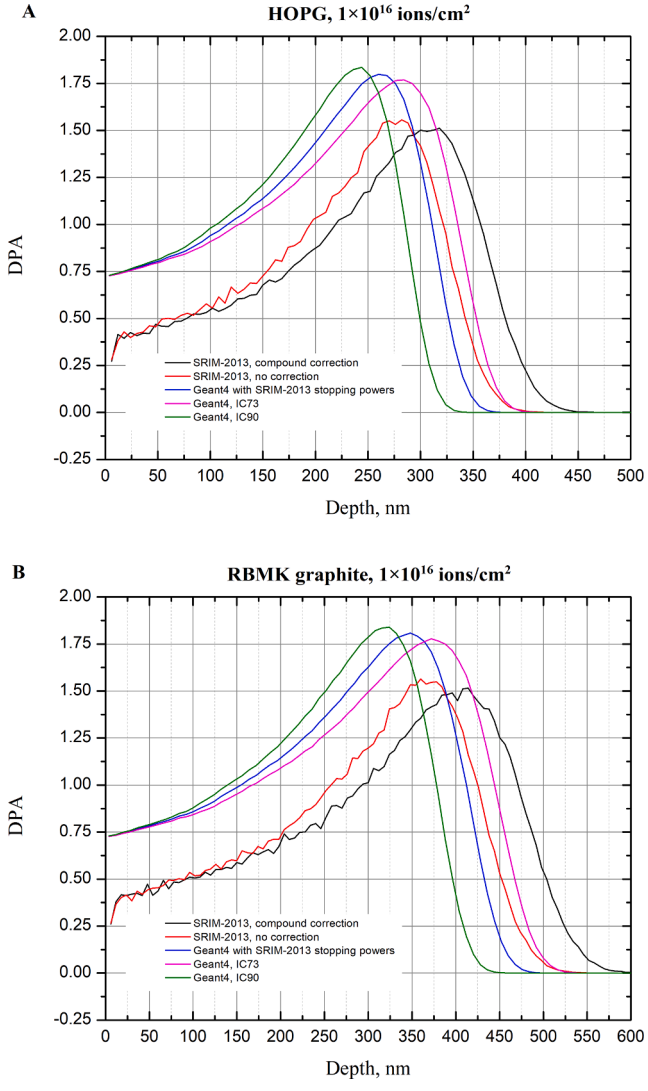

Fig. 4. The implantation induced primary displacement damage (DPA) profiles for both (A) HOPG and (B) RBMK graphite evaluated by using GEANT4 and SRIM-2013 codes at 1 × 10^{16} ions/cm^2.

displacement damage, difference between peak maxima positions is around 75 nm in HOPG, and around 90 nm in RBMK graphite. GEANT4 predicts more displacements closer to the sample surface than SRIM-2013.

When simulating ion implantation profiles with GEANT4, a difference in the final distribution of the ions is observed when different stopping powers/parametrizations are used. The ICRU90 stopping tables gives a narrower distribution with the projected range and peak maximum being by 20–30 nm lower than the one obtained with SRIM-2013 and GEANT4 with SRIM stopping powers. When SRIM stopping powers are used in GEANT4, the implanted ion profile coincides well with the distribution obtained by using SRIM-2013 without compound correction. When compound correction is used in SRIM-2013, the profile shifts by 30–40 nm to higher depths and a good agreement with the GEANT4 ICRU73 approach is observed. With higher projected range values, a clear spread of the distribution by depth is observed. Thus, the simulated profile of implanted ions depends significantly on the stopping powers used. As comparison of stopping powers and different methods were not the main focus of the paper, the different approaches were used to estimate the most expected depth of primary displacement damage and implanted ion maxima.

3.3. *Raman spectroscopy and optical microscopy analysis*

The typical Raman spectrum of carbonaceous material exhibits two characteristic peaks: the G peak at 1580 cm^{-1} and the D peak at around 1350 cm^{-1} (in case of excitation light of 532 nm). The G band (E_{2g} symmetry) represents the C=C stretching modes and indicates the sp^2 hybridization. This mode is always allowed in the Raman spectrum of graphite. The D band (A_{1g} symmetry) is Raman-forbidden mode in perfect graphite and it becomes active due to structural imperfections, impurities, and disorders [24,25]. In case of highly disordered structure the D'' band with peak at around 1500 cm^{-1} is found in between of the G and D bands. This broad band shows the presence of amorphous carbon [26]. At the high frequency side of G band (near 1620 cm^{-1} the defect-induced band D' can be observed [26,27]. Analysis of relative intensity of this band allows to probe the nature of defects [27]. The Raman spectra are shown in Fig. 5 for HOPG (A) and RBMK (B) for both fluences and temperatures. All spectra are normalized in relation to the symmetry-allowed G band. These results are in agreement with those of Ammar et al. [28] obtained in HOPG implanted with ^{37}Cl ions at 10^{16} ions cm^{-2}.

When comparing HOPG and nuclear grade RBMK graphite, several differences should be noted, consistent with those observed when comparing HOPG with the French UNGG nuclear graphite [28]. The spectrum of raw HOPG shows the absence of the D band due to the ideal

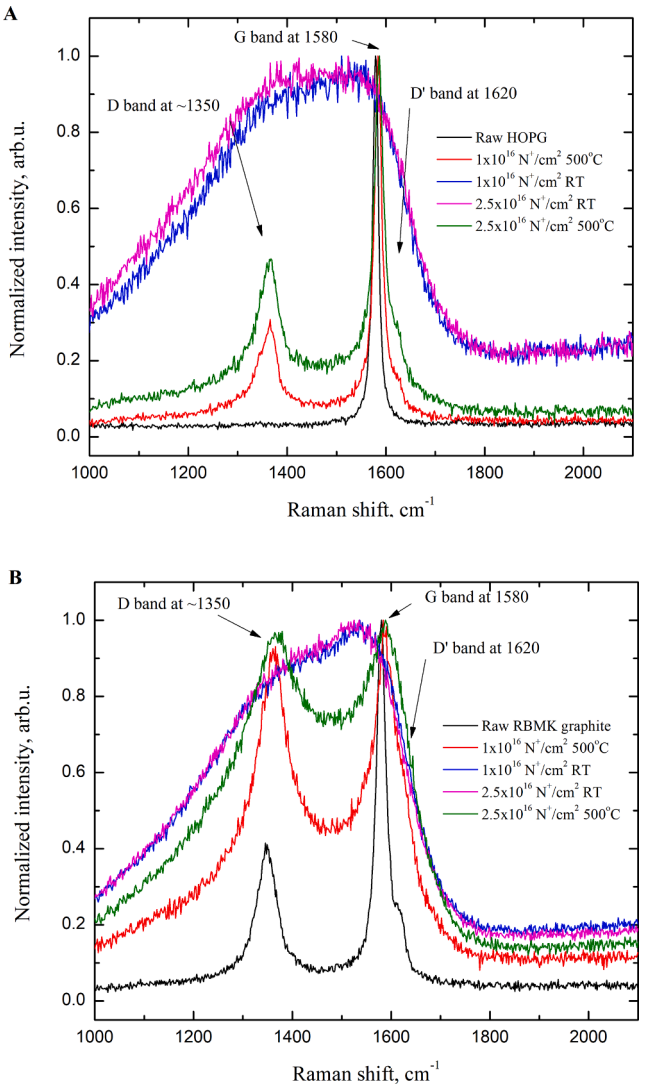

Fig. 5. Raman spectra of HOPG (A) and RBMK (B) graphite samples – raw and implanted with 1.0 or 2.5 × $10^{16}N^+/cm^2$ at RT or 500 °C.

hexagonal structure of the graphene sheets as well as correct interplanar stacking of them. The spectrum of the non-irradiated RBMK graphite, contrary to HOPG, exhibits the presence of the D band. Similar observations were also observed in case of UNGG graphite [28]. The nuclear grade graphite contains grains and pores, which leads to non-uniformities on the surface after sample preparation procedures. Previous studies showed that the samples with the cleaved surface demonstrate the lowest intensity of D band compared to ones treated according to other sample preparation techniques [6]. However, as mentioned previously, in this research the samples were cut-off in order to expose the smooth surface for uniform ion implantation as well as proper SIMS profile measurements. The disorder parameters of the cut-off samples are higher when compared to the cleaved ones, though they still match the features of the unirradiated polycrystalline nuclear graphite which are reported as FWHM<20 cm^{-1} and the I_D/I_G ratio below 1 [29].

The Raman spectra of both HOPG and RBMK graphite samples implanted at the RT show that D and G bands overlap with each other indistinguishably for both fluences of 1.0 × 10^{16} ions/cm^2 and 2.5 × 10^{16} ions/cm^2. In these cases the surfaces of the graphite samples are almost fully amorphous, however, as previous studies have shown, the highly amorphous graphite structure could be reordered if appropriate temperature treatment is applied [6]. If some areas exhibiting patterns of microcrystalline graphite remain in very heavily damaged regions, they can initiate the crystalline regrowth under appropriate annealing conditions [30].

Although similar trends in increase of the D band intensity in both HOPG and RBMK graphite samples are observed, the latter exhibits higher morphological disorder at microscopic level and stronger amorphization than HOPG. On the other hand, the surfaces of RBMK graphite samples remained without any visually observable changes. The HOPG samples exhibited different macrostructural behavior depending on irradiation conditions. Fig. 6 presents optical microscopy images of HOPG sample surfaces irradiated at different ion fluencies at both RT and 500 °C temperature.

At RT the surface of HOPG graphite samples exhibits visually observable fractures, which are significant on the surface of the sample implanted at a fluence of 2.5 × 10^{16} ions/cm^2, while the sample implanted at a fluence of 1 × 10^{16} ions/cm^2 is less fractured. At the temperature of 500 °C, the sample surface remains intact. According to the detailed studies on surface damage of the crystalline graphite due to the ion implantation, the cracks are initiated at a grain boundary and they propagate along grain boundaries. As they propagate, the cracks join other cracks to form polygons when the crack length l_c is comparable to the grain boundary dimensions [30]. Similar observations were reported by Watanabe et al. [31,32]. The appearance of cracks is attributed to the increase of the surface strain, which is induced by formation of amorphous carbon also known as diamond-like carbon (DLC) in the sample surface layer exposed to N^+ implantation.

This is also consistent with the SIMS experiments. No broadening of the depth profiles is observed after the implantation at 500 °C which means that no nitrogen diffusion is occurring in our conditions. However, a small shift towards the surface of the depth profiles maximum is always observed after implantation at 500 °C, at a depth which is roughly the maximum of the damage depth profile calculated by the Monte Carlo codes. The Raman analysis clearly show that the damage created by the implantation process is limited due to the temperature or that the annealing occurs quickly after the collision cascades preventing the formation of defect clusters. In all cases, there is a limited mobility of the defects which can be associated to this short-range movement of N atoms seen by SIMS.

In case of RBMK type reactor the maximum calculated graphite temperature is 750 °C, however, the average temperature of the graphite stack during operation is about 500 °C [33]. The current experiment revealed that during the dynamical annealing of the graphite structure at the operating RBMK-1500 reactor temperature, most of the $^{14}N(n, p)^{14}C$ reaction dependent ^{14}C is immobilized in the graphite matrix. This suggests that the graphite matrix is a highly effective ^{14}C migration barrier, which is one of the determining factors for the assessment of the final disposal strategy.

4. Conclusions

The study on morphological changes and temperature effects on both ion migration and structural disorder level in the HOPG and RBMK nuclear grade graphite samples was carried out by using the 180 keV $^{14}N^+$ ion implantation at the fluences of 1.0 × 10^{16} ions/cm^2 and 2.5 × 10^{16} ions/cm^2 under RT and 500 °C.

- Experimentally by SIMS obtained nitrogen profiles are in good agreement with simulated ones. Comparing the GEANT4 and SRIM-2013 simulation data, the maximum range position varies less for HOPG than for RBMK graphite. Moreover, it should be noted that for RBMK graphite the experimental nitrogen profiles are much broader than simulated ones. SRIM-2013 modelling results are in better agreement with experimental data, when comparing with GEANT4 and further studies are needed to obtain the more accurate prediction. However, GEANT4 could be also used considering the possible discrepancies.

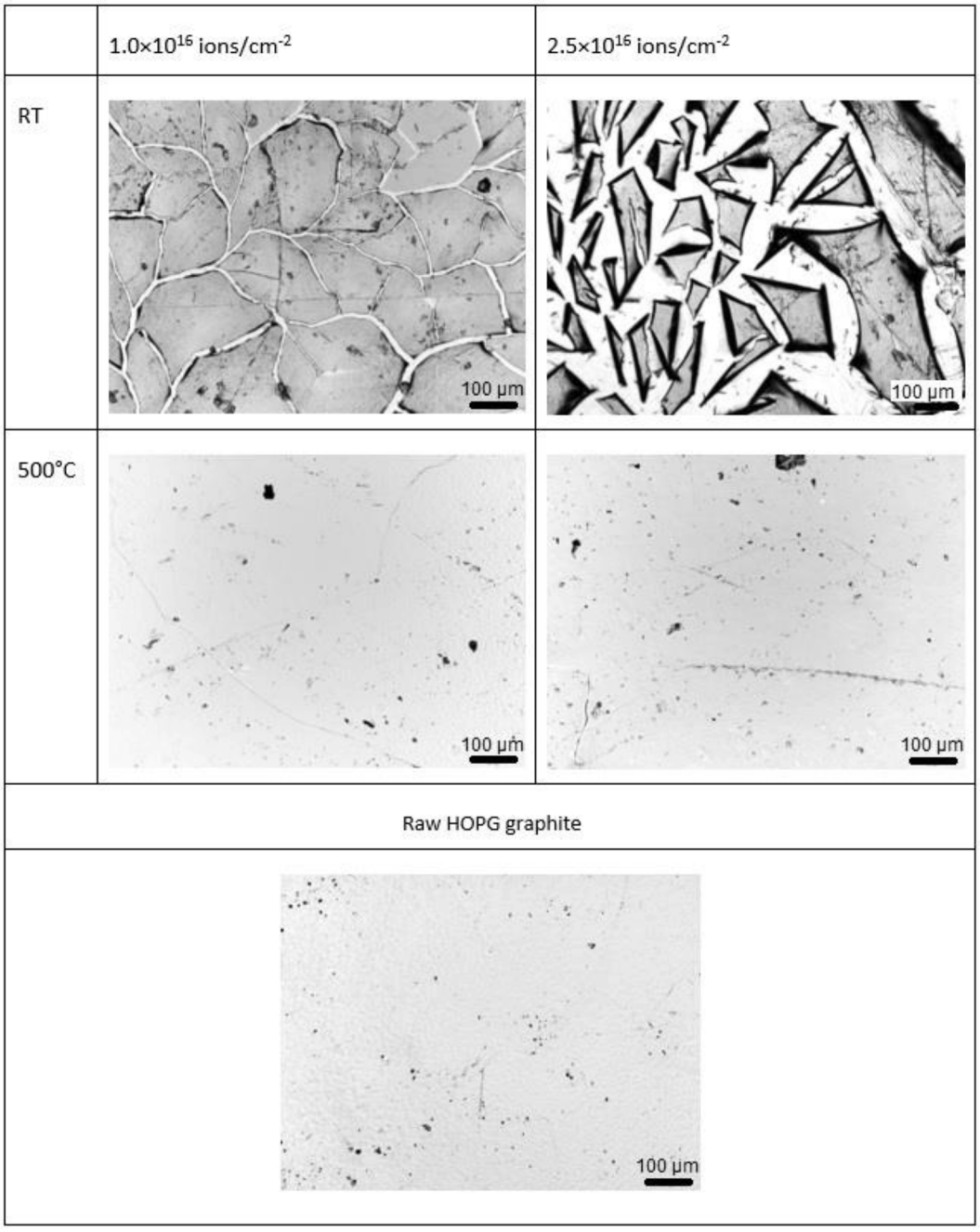

Fig. 6. The surface state of the HOPG samples implanted at different ion fluences and temperature conditions. Scale – 100 μm.

- $^{14}N^{+}$ ion damage indicates that nitrogen is more mobile in the porous RBMK nuclear grade graphite structure compared to monocrystalline – but in both cases only the slight shift of the nitrogen profile maximum to the sample surface is observed when implanted at 500 °C.
- Based on the Raman spectra, the dynamical annealing of defects during implantation is more effective than defect annealing after implantation process is finished. Displacement damage induced by ion implantation process creates point defects and if they are simply annealed during implantation process, the formation of complex defects does not occur.
- Operational temperature of nuclear reactor (~350–550 °C) is high enough to ensure that both defect creation and structural reordering process occur at the same time. Due to this, the full amorphization of the crystal matrix is avoided and the functional properties of graphite are not lost, which ensures proper functionality of the material.
- During the dynamical annealing of the graphite structure in the operating RBMK-1500 reactor, most of the $^{14}N(n,p)^{14}C$ reaction dependent ^{14}C is immobilized in the graphite lattice. This analysis of ^{14}C behaviour in RBMK graphite suggests that the graphite matrix is a highly effective ^{14}C dispersion barrier, which is one of the determining factors in the assessment of the surface/geological storage choice strategy.

CRediT authorship contribution statement

Elena Lagzdina: Conceptualization, Methodology, Formal analysis, Visualization, Writing – original draft, Project administration. **Danielius Lingis:** Software, Validation, Data curation, Formal analysis, Visualization, Writing – review & editing. **Yves Pipon:** Methodology, Formal analysis, Software, Validation, Writing – review & editing. **Rita Plukienė:** Conceptualization, Validation, Project administration, Writing – review & editing. **Ilja Ignatjev:** Methodology. **Artūras Plukis:** Conceptualization, Methodology. **Nathalie Moncoffre:** Conceptualization, Methodology, Resources, Writing – review & editing, Supervision. **Gediminas Niaura:** Resources, Writing – review & editing, Supervision. **Vidmantas Remeikis:** Conceptualization, Resources, Project administration, Supervision.

Declaration of Competing Interest

The authors declare the following financial interests/personal relationships which may be considered as potential competing interests: Elena Lagzdina reports financial support was provided by Research Council of Lithuania. Elena Lagzdina reports financial support was provided by Campus France.

Data availability

Data will be made available on request.

Acknowledgements

This project has received funding from European Social Fund (project No 09.3.3-LMT-K-712-14-0112) under grant agreement with the Research Council of Lithuania (LMTLT). Financial support and technical assistance were also received from Campus France and Institut français de Lituanie (Grant n° 942172F). Many thanks to Marc Marteau from Pprime Institute for carrying out the ion implantation procedures. Special thanks to Julien Amalric and Delphine Pavon from SERMA Technologies/*Science et Surface* Laboratory for helpful discussions about SIMS measurements. Many thanks to Tomas Rakickas and Martynas Gavutis from Center for Physical Sciences and Technology, Vilnius, Lithuania for optical microscopy images. Also, special thanks to Philippe Sainsot from INSA Lyon for his help with interferometry measurements as well as to Nelly Toulhoat for the fruitful discussions.

References

[1] D. Vulpius, K. Baginski, C. Fischer, B. Thomauske, Location and chemical bond of radionuclides in neutron-irradiated nuclear graphite, J. Nucl. Mater. 438 (2013) 163–177, https://doi.org/10.1016/j.jnucmat.2013.02.027.

[2] R. Plukienė, E. Lagzdina, L. Juodis, A. Plukis, A. Puzas, R. Gvozdaitė, V. Remeikis, Z. Révay, J. Kučera, D. Ancius, D. Ridikas, Investigation of impurities of RBMK graphite by different methods, Radiocarbon 60 (2018) 1861–1870, https://doi.org/10.1017/RDC.2018.93.

[3] B. Zlobenko, B. Shabalin, V. Skripkin, Y. Fedorenko, V. Yatzenko, Report on graphite categories in the RBMK reactor (D5.3) Version 2, CArbon-14 Source Term CAST Project. (2016).

[4] A.N. Jones, G.N. Hall, M. Joyce, A. Hodgkins, K. Wen, T.J. Marrow, B.J. Marsden, Microstructural characterisation of nuclear grade graphite, J. Nucl. Mater. 381 (2008) 152–157, https://doi.org/10.1016/j.jnucmat.2008.07.038.

[5] G.S. Was, Z. Jiao, E. Getto, K. Sun, A.M. Monterrosa, S.A. Maloy, O. Anderoglu, B. H. Sencer, M. Hackett, Emulation of reactor irradiation damage using ion beams, Scr. Mater. 88 (2014) 33–36, https://doi.org/10.1016/j.scriptamat.2014.06.003.

[6] E. Lagzdina, D. Lingis, A. Plukis, R. Plukienė, M. Gaspariūnas, I. Matulaitienė, V. Kovalevskij, G. Niaura, V. Remeikis, Structural investigation of RBMK nuclear graphite modified by 12C+ ion implantation and thermal treatment, Nucl. Instrum. Methods Phys. Res. B. 444 (2019) 23–32, https://doi.org/10.1016/j.nimb.2019.01.049.

[7] N. Galy, N. Toulhoat, N. Moncoffre, Y. Pipon, N. Bérerd, M.R. Ammar, P. Simon, D. Deldicque, P. Sainsot, Ion irradiation to simulate neutron irradiation in model graphites: Consequences for nuclear graphite, Nucl. Instrum. Methods Phys. Res. B. 409 (2017) 235–240, https://doi.org/10.1016/j.nimb.2017.05.056.

[8] N. Galy, N. Toulhoat, N. Moncoffre, Y. Pipon, N. Bérerd, M.R. Ammar, P. Simon, D. Deldicque, P. Sainsot, Ion irradiation used as surrogate of neutron irradiation in graphite: Consequences on14C and36Cl behavior and structural evolution, J. Nucl. Mater. 502 (2018) 20–29, https://doi.org/10.1016/j.jnucmat.2018.01.058.

[9] D. Lingis, E. Lagzdina, A. Plukis, R. Plukienė, V. Remeikis, Evaluation of the primary displacement damage in the neutron irradiated RBMK-1500 graphite, Nucl. Instrum. Methods Phys. Res. B. 436 (2018) 9–17, https://doi.org/10.1016/j.nimb.2018.08.038.

[10] R.G. Wilson, SIMS quantification in Si, GaAs, and diamond - an update, Int. J. Mass Spectrom. Ion Process. 143 (1995) 43–49, https://doi.org/10.1016/0168-1176(94)04136-U.

[11] S. Agostinelli, J. Allison, K. Amako, J. Apostolakis, H. Araujo, P. Arce, M. Asai, D. Axen, S. Banerjee, G. Barrand, F. Behner, L. Bellagamba, J. Boudreau, L. Broglia, A. Brunengo, H. Burkhardt, S. Chauvie, J. Chuma, R. Chytracek, G. Cooperman, G. Cosmo, P. Degtyarenko, A. Dell'Acqua, G. Depaola, D. Dietrich, R. Enami, A. Feliciello, C. Ferguson, H. Fesefeldt, G. Folger, F. Foppiano, A. Forti, S. Garelli, S. Giani, R. Giannitrapani, D. Gibin, J.J. Gómez Cadenas, I. González, G. Gracia Abril, G. Greeniaus, W. Greiner, V. Grichine, A. Grossheim, S. Guatelli, P. Gumplinger, R. Hamatsu, K. Hashimoto, H. Hasui, A. Heikkinen, A. Howard, V. Ivanchenko, A. Johnson, F.W. Jones, J. Kallenbach, N. Kanaya, M. Kawabata, Y. Kawabata, M. Kawaguti, S. Kelner, P. Kent, A. Kimura, T. Kodama, R. Kokoulin, M. Kossov, H. Kurashige, E. Lamanna, T. Lampén, V. Lara, V. Lefebure, F. Lei, M. Liendl, W. Lockman, F. Longo, S. Magni, M. Maire, E. Medernach, K. Minamimoto, P. Mora de Freitas, Y. Morita, K. Murakami, M. Nagamatu, R. Nartallo, P. Nieminen, T. Nishimura, K. Ohtsubo, M. Okamura, S. O'Neale, Y. Oohata, K. Paech, J. Perl, A. Pfeiffer, M.G. Pia, F. Ranjard, A. Rybin, S. Sadilov, E. Di Salvo, G. Santin, T. Sasaki, N. Savvas, Y. Sawada, S. Scherer, S. Sei, V. Sirotenko, D. Smith, N. Starkov, H. Stoecker, J. Sulkimo, M. Takahata, S. Tanaka, E. Tcherniaev, E. Safai Tehrani, M. Tropeano, P. Truscott, H. Uno, L. Urban, P. Urban, M. Verderi, A. Walkden, W. Wander, H. Weber, J.P. Wellisch, T. Wenaus, D.C. Williams, D. Wright, T. Yamada, H. Yoshida, D. Zschiesche, Geant4—a simulation toolkit, Nucl. Instrum. Methods Phys. Res., Sect. A 506 (3) (2003) 250–303.

[12] J.F. Ziegler, M.D. Ziegler, J.P. Biersack, SRIM – The stopping and range of ions in matter (2010), Nucl. Instrum. Methods Phys. Res. B 268 (2010) 1818–1823, https://doi.org/10.1016/j.nimb.2010.02.091.

[13] R.E. Stoller, M.B. Toloczko, G.S. Was, A.G. Certain, S. Dwaraknath, F.A. Garner, On the use of SRIM for computing radiation damage exposure, Nucl. Instrum. Methods Phys. Res. B. 310 (2013) 75–80, https://doi.org/10.1016/j.nimb.2013.05.008.

[14] R.E. Stoller, M.B. Toloczko, G.S. Was, A.G. Certain, S. Dwaraknath, F.A. Garner, Erratum: (On the use of SRIM for computing radiation damage exposure (2013) 310 (75–80), (S0168583X13005053), (10.1016/j.nimb.2013.05.008)), Nucl. Instrum. Methods Phys. Res. B. 459 (2019) 196–197. https://doi.org/10.1016/j.nimb.2019.08.015.

[15] M.J. Norgett, M.T. Robinson, I.M. Torrens, A proposed method of calculating displacement dose rates, Nucl. Eng. Des. 33 (1975) 50–54, https://doi.org/10.1016/0029-5493(75)90035-7.

[16] J.F. Ziegler, J.M. Manoyan, The stopping of ions in compounds, Nucl. Inst. Methods Phys. Res. B 35 (3-4) (1988) 215–228.

[17] R. Bimbot, H. Geissel, H. Paul, A. Schinner, P. Sigmund, A. Wambersie, P. M. DeLuca, S.M. Seltzer, Stopping of ions heavier than helium, J. ICRU 5 (2005), https://doi.org/10.1093/jicru/ndi001.

[18] ICRU, Key data for ionizing-radiation dosimetry: measurements standards and applications (ICRU Report 90), J. Int. Commiss. Radiat. Units Meas. 14 (2016).

[19] J. Deasy, ICRU Report 49, Stopping Powers and Ranges for Protons and Alph Particles, Med. Phys. 21 (5) (1994) 709–710.

[20] J.F. Ziegler, Comments on ICRU Report No. 49: Stopping Powers and Ranges for Protons and Alpha Particles, Radiat. Res. 152 (2) (1999) 219.

[21] M. Tapajna, P. Noga, J. Kuzmik, Determination of secondary-ions yield in SIMS depth profiling of Si , Mg , and C ions implanted GaN epitaxial layers, (2018). https://doi.org/10.1109/ASDAM.2018.8544657.

[22] E. Lagzdina, D. Lingis, A. Plukis, R. Plukienė, M. Gaspariūnas, I. Matulaitienė, V. Kovalevskij, G. Niaura, V. Remeikis, Structural investigation of RBMK nuclear graphite modified by 12 C + ion implantation and thermal treatment, Nucl. Instrum. Methods Phys. Res. B 444 (2019) 23–32.

[23] P.J. Hacker, G.B. Neighbour, R. Levinskas, D. Milčius, Characterization of Ignalina NPP RBMK Reactors Graphite Characterization of Ignalina NPP RBMK Reactors Graphite Sample preparation, Medziagotyra. (2001). https://doi.org/ISSN 1392 – 1320.

[24] A.C. Ferrari, Raman spectroscopy of graphene and graphite: Disorder, electron-phonon coupling, doping and nonadiabatic effects, Solid State Commun. 143 (2007) 47–57, https://doi.org/10.1016/j.ssc.2007.03.052.

[25] R. Trusovas, G. Račiukaitis, G. Niaura, J. Barkauskas, G. Valušis, R. Pauliukaite, Recent Advances in Laser Utilization in the Chemical Modification of Graphene Oxide and Its Applications, Adv. Opt. Mater. 4 (2016) 37–65, https://doi.org/10.1002/adom.201500469.

[26] R. Trusovas, K. Ratautas, G. Račiukaitis, G. Niaura, Graphene layer formation in pinewood by nanosecond and picosecond laser irradiation, Appl. Surf. Sci. 471 (2019) 154–161, https://doi.org/10.1016/j.apsusc.2018.12.005.

[27] A. Eckmann, A. Felten, A. Mishchenko, L. Britnell, R. Krupke, K.S. Novoselov, C. Casiraghi, Probing the nature of defects in graphene by Raman spectroscopy, Nano Lett. 12 (2012) 3925–3930, https://doi.org/10.1021/nl300901a.

[28] M.R. Ammar, N. Galy, J.N. Rouzaud, N. Toulhoat, C.E. Vaudey, P. Simon, N. Moncoffre, Characterizing various types of defects in nuclear graphite using Raman scattering: Heat treatment, ion irradiation and polishing, Carbon N Y. 95 (2015) 364–373, https://doi.org/10.1016/j.carbon.2015.07.095.

[29] A.N. Jones, L. McDermott, B.J. Marsden, The Characterization of Irradiation Damage in Reactor Graphite Using High Resolution Transmission Electron

Microscopy and Raman Spectroscopy, MRS Proc. 1475 (2012) 101–106, https://doi.org/10.1557/opl.2012.561.
[30] M.S. Dresselhaus, R. Kalish, Ion Implantation in Diamond, Graphite and Related Materials, Springer Berlin Heidelberg, Berlin, Heidelberg, 1992. https://doi.org/10.1007/978-3-642-77171-2.
[31] H. Watanabe, K. Takahashi, M. Iwaki, Structural characterization of ion implanted HOPG and glass-like carbon by laser Raman spectroscopy, Nucl. Inst. Methods Phys. Res. B 80–81 (1993) 1489–1493, https://doi.org/10.1016/0168-583X(93)90827-S.
[32] H. Watanabe, K. Takahashi, M. Iwaki, Structural characterization of ion implanted pyrolytic graphite, Nucl. Instrum. Methods Phys. Res. B. 257 (2007) 549–553, https://doi.org/10.1016/j.nimb.2007.01.084.
[33] K. Almenas, A. Kaliatka, E. Uspuras, Ignalina RBMK-1500 A Source Book, Lithuanian Energy Institute, 1998., (n.d.).